AGU PUBLICATIONS

JGR

Journal of Geophysical Research: Solid Earth

RESEARCH ARTICLE
10.1002/2013JB010546

This article is a companion to *Sultan et al.* [2010], doi:10.1029/2010JB007453.

Key Points:
- Free gas trapped in shallow micro-fractures near the seafloor
- Very low methane concentrations above the top of the gas hydrate occurrence zone
- Pockmark formation controlled by rapid hydrate growth and hydrate dissolution

Correspondence to:
N. Sultan,
nabil.sultan@ifremer.fr

Citation:
Sultan, N., et al. (2014), Pockmark formation and evolution in deep water Nigeria: Rapid hydrate growth versus slow hydrate dissolution, *J. Geophys. Res. Solid Earth*, *119*, 2679–2694, doi:10.1002/2013JB010546.

Received 22 JUL 2013
Accepted 13 MAR 2014
Accepted article online 18 MAR 2014
Published online 28 APR 2014

Pockmark formation and evolution in deep water Nigeria: Rapid hydrate growth versus slow hydrate dissolution

N. Sultan[1], G. Bohrmann[2], L. Ruffine[1], T. Pape[2], V. Riboulot[1], J.-L. Colliat[3], A. De Prunelé[1], B. Dennielou[1], S. Garziglia[1], T. Himmler[1,2], T. Marsset[1], C.A. Peters[2], A. Rabiu[4], and J. Wei[2]

[1]Ifremer, REM/GM/LES, Plouzané, France, [2]MARUM - Center for Marine Environmental Sciences, University of Bremen, Bremen, Germany, [3]TOTAL, Pau, France, [4]NIOMR, Victoria Island, Nigeria

Abstract In previous works, it has been suggested that dissolution of gas hydrate can be responsible for pockmark formation and evolution in deep water Nigeria. It was shown that those pockmarks which are at different stages of maturation are characterized by a common internal architecture associated to gas hydrate dynamics. New results obtained by drilling into gas hydrate-bearing sediments with the MeBo seafloor drill rig in concert with geotechnical in situ measurements and pore water analyses indicate that pockmark formation and evolution in the study area are mainly controlled by rapid hydrate growth opposed to slow hydrate dissolution. On one hand, positive temperature anomalies, free gas trapped in shallow microfractures near the seafloor and coexistence of free gas and gas hydrate indicate rapid hydrate growth. On the other hand, slow hydrate dissolution is evident by low methane concentrations and almost constant sulfate values 2 m above the Gas Hydrate Occurrence Zone.

1. Study Area and Main Objective

The investigated area is located in deep water of Nigeria. Bathymetry in the area ranges from 1100 to 1250 m (Figure 1). This area was previously shown to host a field of (sub) circular pockmarks [*Georges and Cauquil*, 2007]. These range in shape from a slightly depressed, hummocky seafloor to a much more pronounced depression and each of them is several tens to a few hundreds of meters wide (Figure 1). The various morphologies of the pockmarks suggest either distinct modes of formation or different evolutionary stages [*Sultan et al.*, 2010]. Most of the pockmarks are located in an area bounded by two NW-SE trending deep-rooted normal faults, which delineate a graben linked to the axis of anticline in the subsurface. Several deep and shallow faults and three N-S trending buried channels were recognized with high-resolution 3-D seismic data (Figure 1). The buried channels, which are situated between 80 ms and 180 ms (two-way travel time, TWTT) below the seabed, may have the potential of accumulating amounts of free gas and play therefore an important role for the gas hydrate distributions.

Based on geophysical and sedimentological data, and in situ piezocone measurements, *Sultan et al.* [2007] have shown that pockmark-associated gas hydrate accumulated within a few meters thick sediment layers at shallow depth. In addition, *Sultan et al.* [2010] proposed that the formation of a circular depression around the gas hydrate occurrence zone (GHOZ) is related to multiple steps in the pockmark evolution. The sequence is starting with hydrate formation induced by upward migration of fluids oversaturated in gas through fracture systems followed by decrease of fluid flow resulting in gas undersaturation, hydrate dissolution, generation of excess pore pressure, and by concurrent collapse of the gas hydrate-bearing sediment structures. Respective analyses were mainly based on subseabed approaches, using piston cores and in situ piezocone geotechnical measurements with a maximum penetration of 30 m below seafloor (mbsf). However, the gas hydrate stability zone (GHSZ) in this area is expected to expand from 90 to 120 mbsf [*Sultan et al.*, 2010, Figure 20] and several relatively deep structures (buried channels, microfaults and fractures) and intermediate reservoirs are located below the previously investigated shallow subseabed area.

In order to better understand processes that control not only the formation but also the evolution of pockmarks, longer cores of gas hydrate-bearing sediments were drilled using the MeBo seafloor drill rig [*Freudenthal et al.*, 2009] during the French-German Guineco-MeBo expedition in December 2011 on board

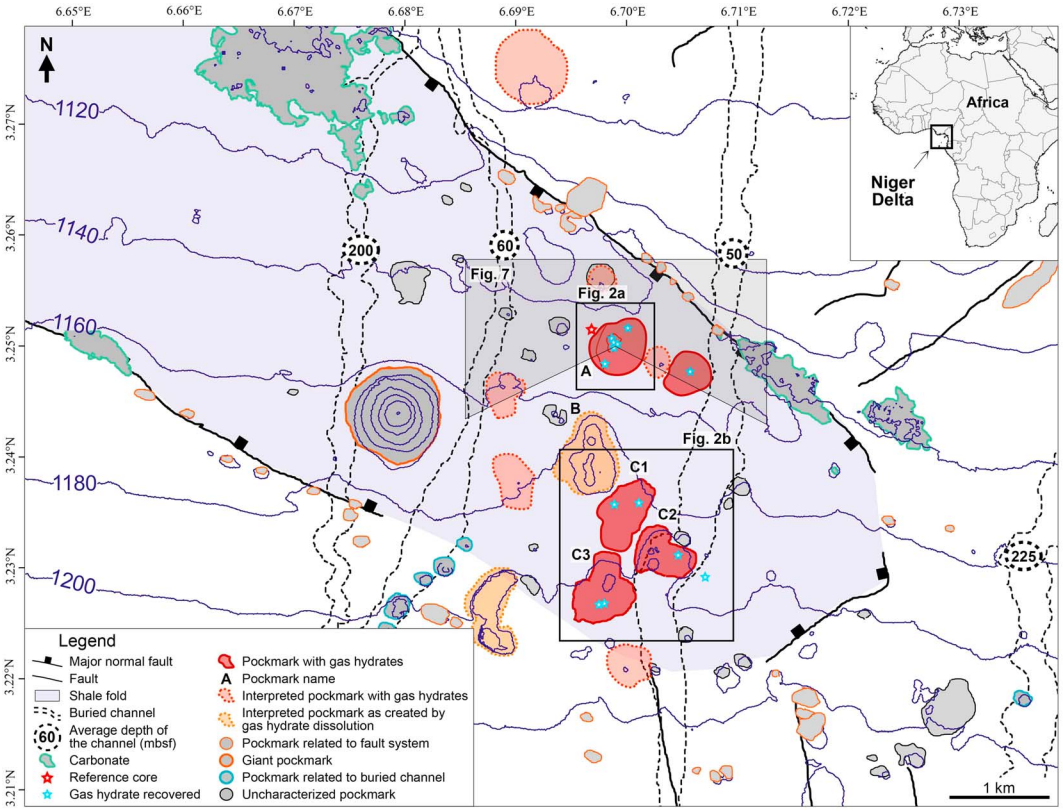

Figure 1. Interpreted bathymetry map of the study area based on industrial AUV data [*Georges and Cauquil*, 2007] showing studied pockmarks (pockmark A to the north and pockmarks C1, C2, and C3 to the south). Deep buried channels (between 80 and 100 ms TWT below seabed) are projected on the bathymetric map (dashed lines). Most pockmarks are located within a NW-SE trending area bounded by two deep-rooted normal faults clearly expressed on the bathymetric map.

the French research vessel "Pourquoi Pas?." The MeBo drill rig enabled recovery of sediments down to approximately 57 mbsf which markedly upgrades the previously acquired data set. Based on newly acquired data, this paper aims at providing the founding elements to answer whether pockmark morphology is related to the stage of evolution and/or distinct modes of pockmark formation. The present research works serve as a companion paper to our previous paper on the "hydrate dissolution as a potential mechanism for pockmark formation in the Niger delta" [*Sultan et al.*, 2010]. In the following and based on key indices, it will be demonstrated that the main process controlling gas hydrate formation and pockmark evolution is dynamic gas inflows and outflows which are controlled by rapid and episodic hydrate growth versus slow hydrate dissolution.

2. Acquired Data

During the Guineco-MeBo expedition a multidisciplinary approach was used, comprising geology, sedimentology, geochemistry and geotechnics, and applying various sampling and measurements tools. Sediment cores were retrieved by means of the MeBo seafloor drill rig, a ship-based Kullenberg-type piston corer (Ifremer Jumbo Calypso corer), a gravity corer, and the pressure-tight Dynamic Autoclave Piston Corer (DAPC). Using MeBo, up to 57 m long sediment cores could be recovered (shown in Figures 2–5). The Ifremer Jumbo Calypso corer and the gravity corer were used to recover shallow sediment samples (Figures 2a and 2b). At selected stations, thermal probes were mounted to the cutting barrel of the gravity corer in order to measure in situ thermal gradients (Figure 2a). The DAPC [*Abegg et al.*, 2008] was used to recover pressurized cores in hydrate-bearing areas of pockmark A (Figure 2a).

The Ifremer Penfeld was used to perform up to 30 m deep piezocone (Figures 2a and 2b) and *P* wave velocity (celerimeter) measurements profiles (Figures 2a and 2b). Finally, the Ifremer piezometer was used to measure

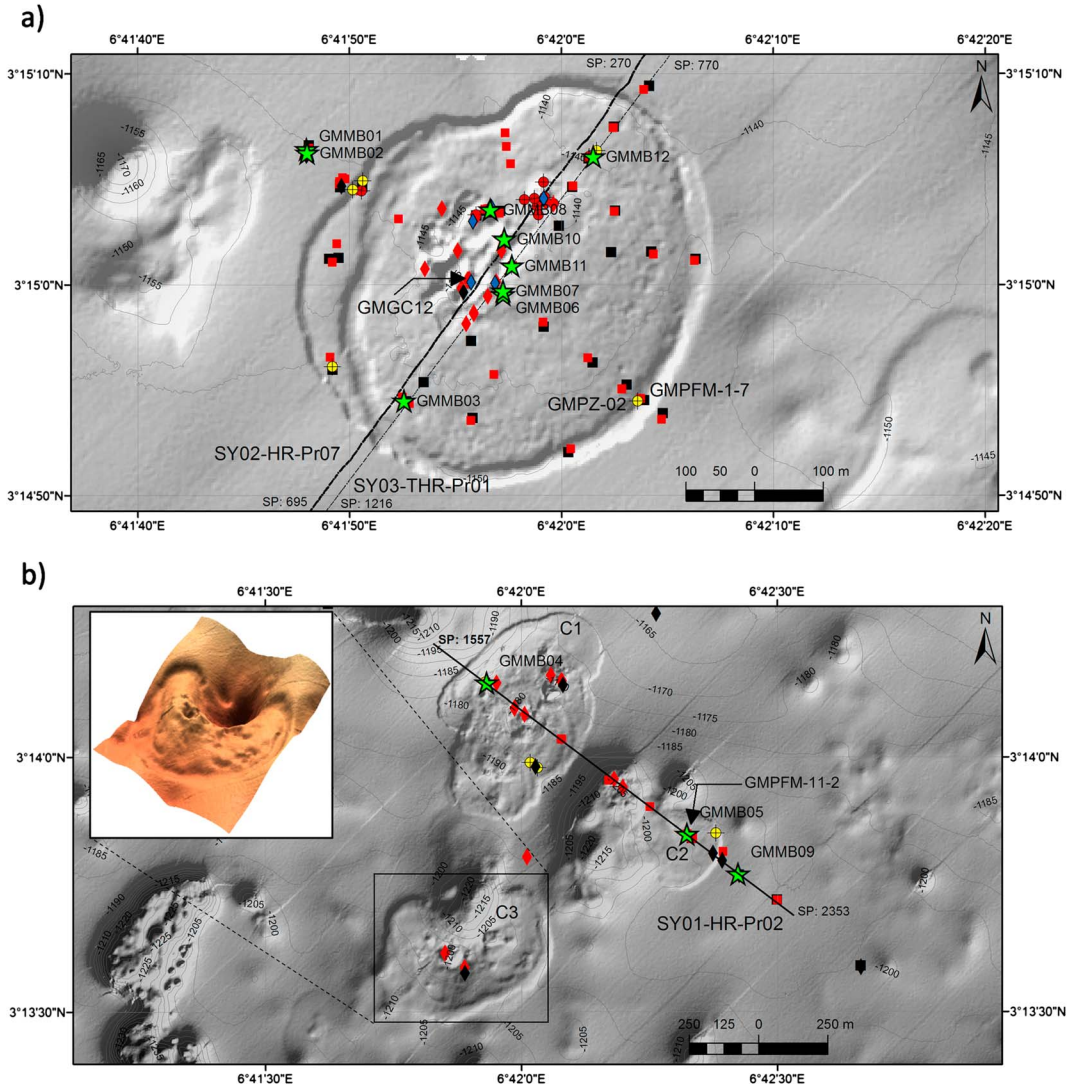

Figure 2. Overview about stations and acquired data. Calypso and gravity cores: blue diamonds; MeBo drills: green stars; Gravity cores with thermal probes: red circle targets; Penfeld piezocone: red squares; Penfeld celerimeter: black squares; Piezometer: yellow circle targets during GM cruise projected on shaded bathymetry maps of (a) pockmark A and (b) pockmarks C1, C2, and C3. Only sites and data used in the present paper are labeled. Locations of SYSIF seismic profiles SY03-THR-PR01, SY02-HR-PR07, and SY01-HR-PR02 and corresponding Shot Point (SP) are also shown. In Figure 2b, a 3-D view of pockmark C3 bathymetry shows the coexistence of two stages of the pockmark going from dome structure to deep depression.

pore pressure and temperature down to 14 mbsf with waiting periods ranging between 6 h and 4 days (Figures 2a and 2b). Data and samples were acquired during the cruise from 15 Calypso cores, 36 gravity cores, 13 gravity cores with temperature measurements, 6 DAPC cores, 12 MeBo deep cores, 52 in situ piezocone measurements, 38 in situ celerimeter measurements, and 10 piezometer deployments.

Measurements of sulfate and chloride concentrations, alkalinity, and pH were carried out on board. Ex situ methane concentrations in pore waters and molecular compositions of hydrate-bound gases were determined. Lithological core descriptions were made on board. An Avaatech X-ray fluorescence core-scanner system was used to perform stepwise (1 cm) analyses of major elements from Al to U on selected core archive halves. In order to identify the key mechanical and physical sediment parameters, an onboard experimental geotechnical program on undisturbed marine sediment samples was undertaken (including the use of the GEOTEK Multi-Sensor Core Logger and shear strength measurements). In order to trace gas hydrate distributions in the sediment, data from continuous infrared thermal core imaging and pore water

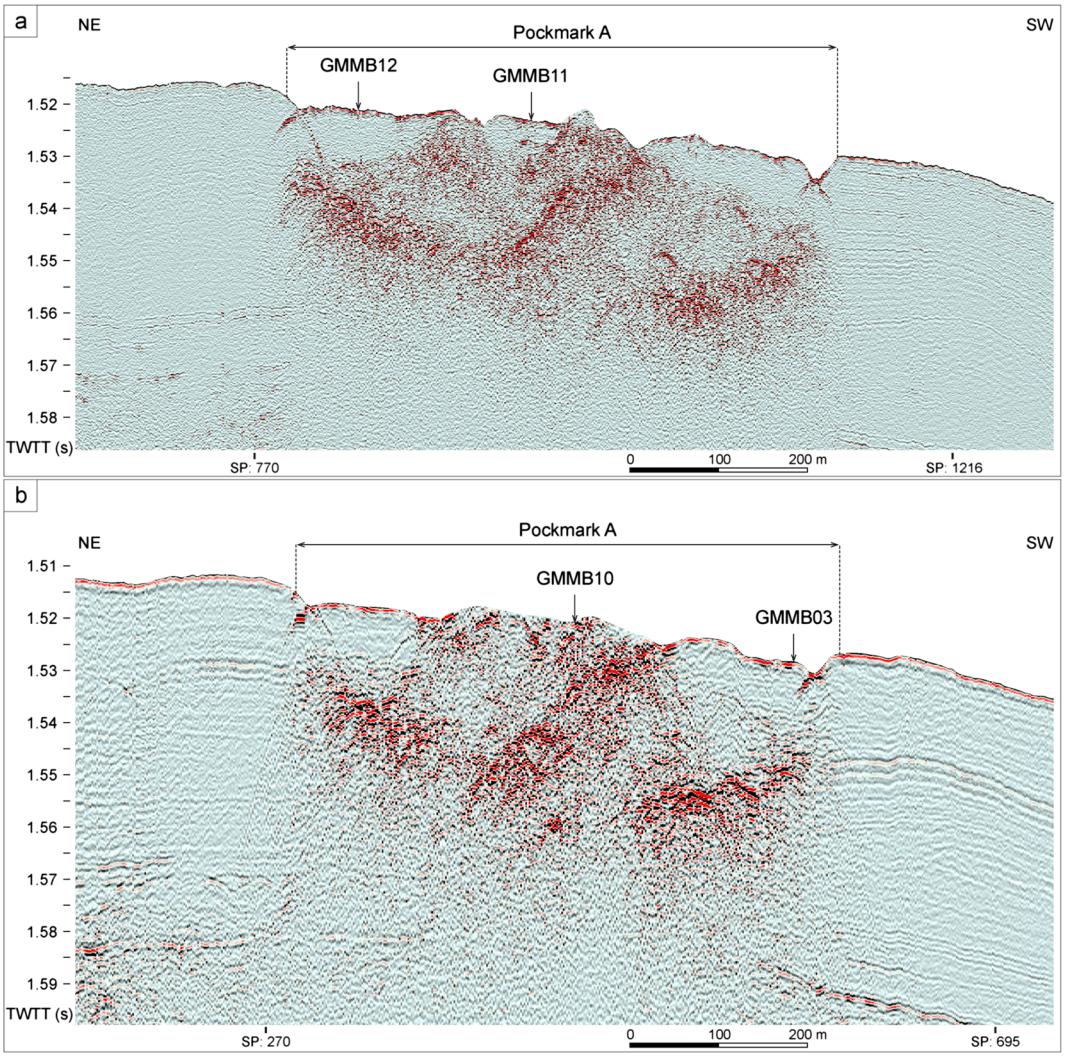

Figure 3. SYSIF seismic profiles (a) SY03-THR-PR01 and (b) SY02-HR-PR07 showing a significant contrast between high-amplitude chaotic facies at the center of pockmark A and low-amplitude subparallel reflectors of surrounding sediments. Four MeBo drill sites are indicated on the seismic lines.

analysis performed before core liner splitting were jointly evaluated with sediment observations. In addition, in situ piezocone geotechnical measurements were used as an indirect indication for the gas hydrate presence. Indeed, gas hydrate is characterized by very high resistance that can be easily detected with the high-corrected cone resistance (qt) recorded during piezocone measurements.

The seismic data used in the present work were acquired during a previous cruise using the Système Sismique Fond (SYSIF) deep towed acquisition system [*Ker et al.*, 2010; *Marsset et al.*, 2010]. SYSIF is a heavy towed apparatus hosting low-frequency acoustic transducers (250–1000 Hz, 650–2000 Hz) and a single channel streamer in order to provide high-resolution (HR) images of the subbottom. The altitude of SYSIF over the seafloor is set to 100 m thus reducing the Fresnel zone, i.e., enhancing the lateral resolution compared to conventional surface towed systems. All those seismic data were not migrated and were already presented in the companion paper [*Sultan et al.*, 2010].

3. Key Mechanisms: Previous Works and New Observations

In the following, the two main processes controlling pockmarks formation and evolution in the area are presented and discussed using background literature, data analysis, and interpretation.

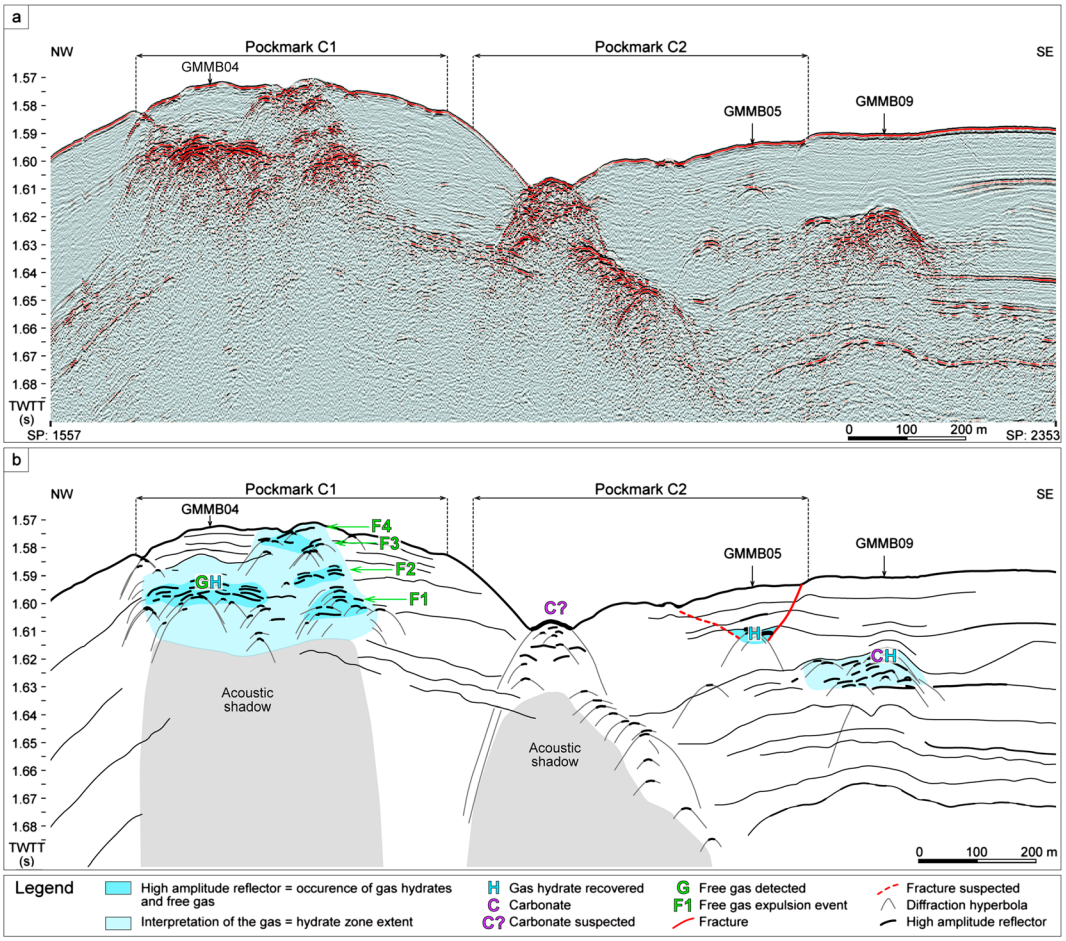

Figure 4. (a) SYSIF SY01-HR-PR02 seismic profile and (b) interpreted profile crossing pockmarks C1 and C2 and indications of MeBo drill sites. The letter G in Figure 4b corresponds to the source of free gas flow generated during MeBo drilling GMMB04. The G fits with a diffraction hyperbola's high-amplitude reflectors preventing a clear detection of the free gas source. On the seismic profile, four reflectors (F1 to F4), which are suspected to result from four natural free gas expulsion events, are indicated. Gas hydrate was recovered from reflector F4 by coring.

3.1. Rapid Hydrate Growth

3.1.1. Coexistence of Free Gas and Gas Hydrate

3.1.1.1. Previous Works and Background

The coexistence of free gas and gas hydrate has been first reported from the Oregon continental margin where ascending saline fluids may lead to a local shift in the gas hydrate stability toward less stable conditions, thereby allowing movement of free gas through the GHSZ [*Trehu et al.*, 2003; *Milkov et al.*, 2004; *Torres et al.*, 2004; *Liu and Flemings*, 2006]. The absence of pore water in sufficient amounts can be an additional cause for the presence of free gas in gas hydrate-bearing sediments [*Lee and Collett*, 2006]. Based on seismic data and in situ *P* wave velocity measurements, free gas and gas hydrate were already suspected to co-occur widespread in the present study area [*Sultan et al.*, 2007].

3.1.1.2. New Acquired Data and Observations

Newly acquired data and mainly coring confirmed the coexistence between free gas and gas hydrate. Highly porous gas hydrate recovered from shallow sediments at the central part of pockmark A (gravity corer GMGC12 in Figure 2a) shows the presence of free gas alveoli isolated in massive gas hydrate (Figure 6a). The pore size of a unit gas alveolus is 2 to 3 mm in diameter. The gas hydrate sample in Figure 2a was recovered from the interval 1 to 2 mbsf.

3.1.1.3. Interpretation

The complete isolation of gas alveoli in the sediment can be explained by rapid injection of gas-rich fluids along fractures into the GHSZ. As a consequence, rapid gas flux results in rapid gas hydrate accumulation

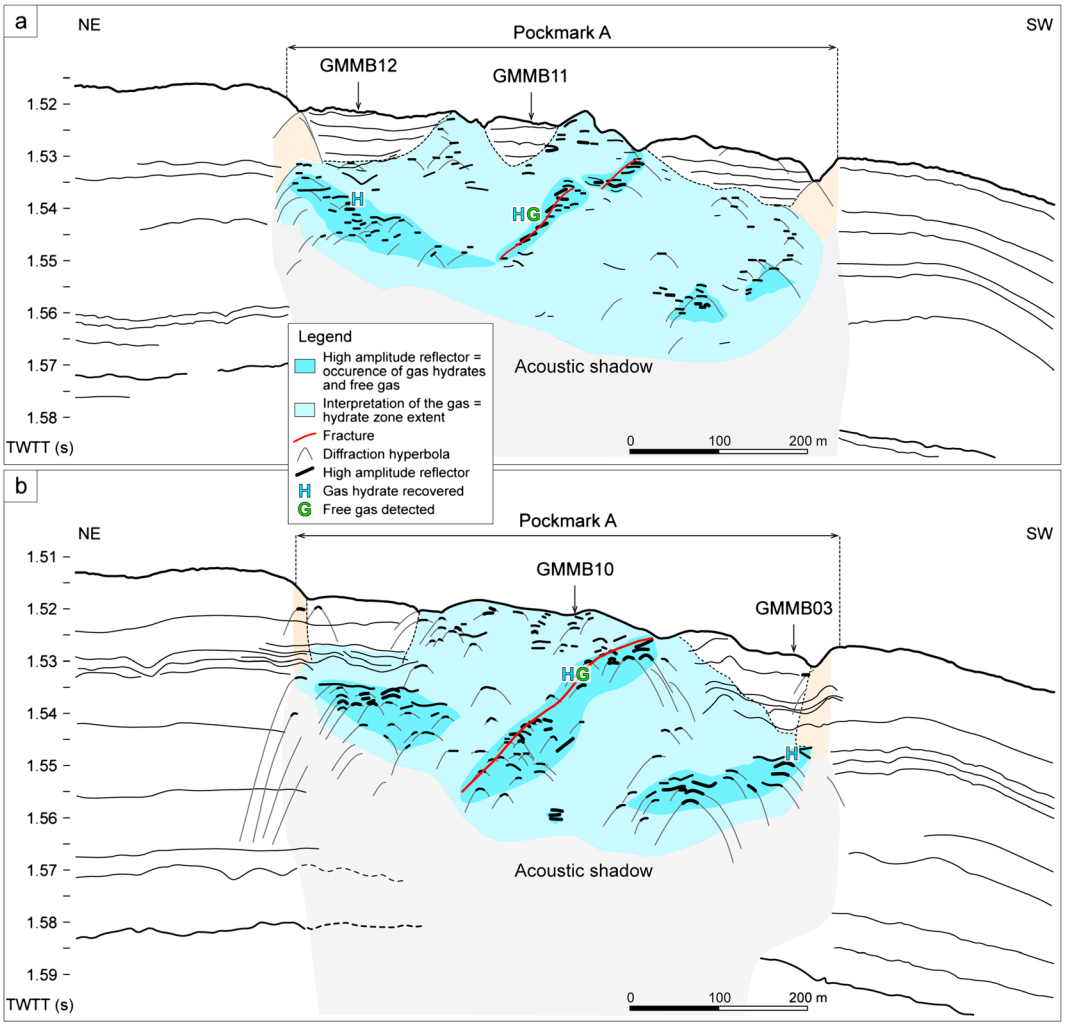

Figure 5. Interpreted SYSIF seismic profiles (a) SY03-THR-PR01 and (b) SY02-HR-PR07 and indications of MeBo drill sites at pockmark A. The letter G corresponds to the sources of free gas flow generated during MeBo drillings after crossing hydrate layers (letter "H"). For GMMB11 and GMMB10, the two Gs fit well with shallow subseabed fractures.

which may isolate free gas zones (i.e., gas-filled pores) from the surrounding pore water. The preservation of those free gas zones can be explained by the very low permeability of gas hydrate for water and gas.

3.1.2. Free Gas in the Water Column Above Pockmark A

3.1.2.1. Previous Works and Background

Gas plumes in the seawater above gas-bearing and gas hydrate-bearing sediments are frequent [e.g., *Paull et al.*, 1995; *Roemer et al.*, 2012]. For instance, *Paull et al.* [1995] reported gas plumes crossing the GHOZ over the Blake Ridge and *Taylor et al.* [2000] suggested that these gas plumes are related to high-pore water salinity. For seep sites in the south-eastern Black Sea, *Pape et al.* [2011] suggested that constant fluid supply from greater depth leads to overpressure in free gas accumulation zones beneath a continuous shallow hydrate layer which may cause hydrate detachment from the seafloor and buoyant rise through the water column.

3.1.2.2. New Acquired Data and Observations

Two hydroacoustic anomalies caused by rising gas bubbles (plumes) of naturally escaping free gas in the central part of pockmark A have been detected during the cruise by the vessel multibeam echosounder (Seabat 7150). The gas plumes disappeared from the records around 500 m above seabed (i.e., 600 mbsl) (Figure 6b). Repeated acoustic water column scanning above the whole study zone (around 40 km^2) during the expedition confirmed (1) continuous natural seepage of free gas from the central part of pockmark A and (2) the absence of other plumes in the area.

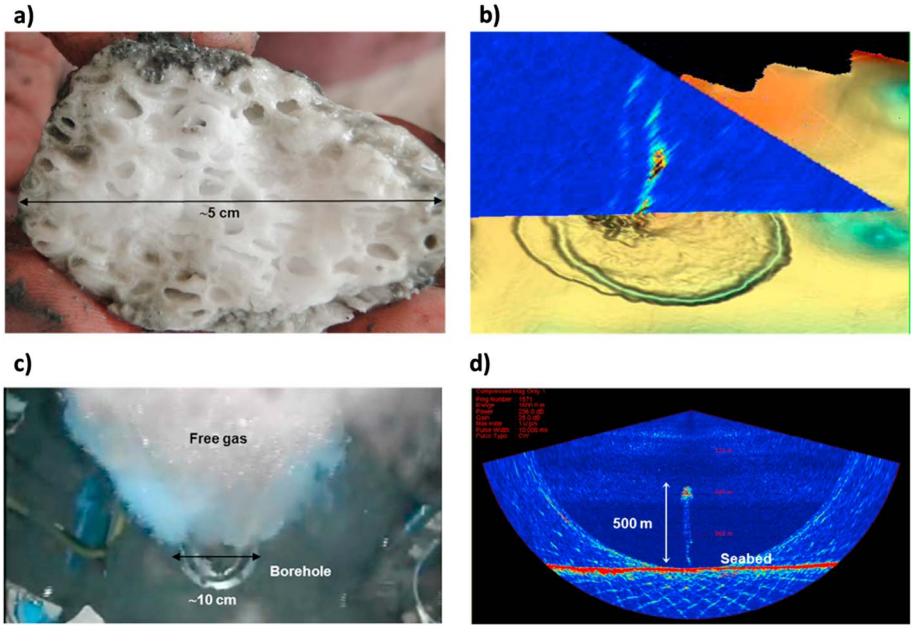

Figure 6. (a) Photograph of a porous hydrate specimen recovered from the central part of pockmark A (GMGC12 in Figure 2a) showing the possible coexistence between gas hydrate and free bubble-forming gas. (b) Two gas plumes sources in the central part of pockmark detected, thanks to the multibeam echosounder (SeaBat 7150). (c) Gas flow from a source at around 18 mbsf (site GMMB04—high amplitude in Figure 4b indicated by "GH") as recorded by the MeBo camera (Marum) during drilling and (d) the detection with the multibeam echosounder of the gas flow generated during drilling (site GMMB04). Gas plumes were dispersed completely 500 m above the seabed (around 600 m below the sea surface).

3.1.2.3. Interpretation

The source of the gas plumes seems to be spatially associated with the shallow fractures shown in the seismic profiles in Figure 5a and is directly linked to the seismic horizon R previously reported (Figure 7). It is noteworthy that the high-amplitude chaotic facies and the numerous diffraction hyperbolas prevent precise identification of fractures. A three-dimensional view of pockmark A sediments, which was constructed from autonomous underwater vehicle (AUV) bathymetric data and industrial 3-D seismic data, illustrates that the seismic reflector R is associated to a horizon forming a gas storage zone (horizon R, Figure 7) at around 0.3 s (TWT) below the seabed (around 232 mbsf for a mean *P* wave velocity of 1550 m/s). Two other pockmarks to the east and the west of pockmark A are supplied by gas from horizon R as well (Figure 7). The vigorous gas flow through the GHOZ into the overlying water column at the central part of pockmark A provides evidence of growth of shallow gas hydrate fueled by gas ascent from horizon R through fractures toward the seafloor rather than slow diffusion.

3.1.3. Free Gas Within the GHOZ

3.1.3.1. New Acquired Data and Observations

The MeBo targets aimed to drill through gas hydrate layers, in particular through shallow subseabed structures (high-amplitude reflectors, suspected fractures) and well expressed seabed depressions (Figure 2). A free gas accumulation was discovered during MeBo drilling GMMB04 at pockmark C1 (Figures 1 and 4). Having penetrated a relatively thin hydrate layer (marked by a very high amplitude chaotic facies on seismic, see Figure 4) at around 18 mbsf by rotary drilling, vigorous flow of free gas suddenly occurred and significant amounts of gas bubbles escaped from the borehole continuously for more than 1 h (Figure 6c). Drilling torque data show that the thin hydrate layer above the free gas layer was characterized by a relatively high stiffness and cameras from the MeBo filmed pieces of hydrate expulsed from the drilling borehole. This gas discharge from the subseafloor structure to the water column was also detected by the vessel multibeam echosounder (SeaBat 7150) (Figure 6d). It was dispersed completely, as for the case of the natural gas plumes, 500 m above the seabed. Drilling operations were aborted during GMMB-04 because of visibility problems (gas hydrate was formed instantaneously on cameras). Other free gas-pocket zones isolated from surrounding gas hydrate-bearing sediments were discovered during MeBo drillings GMMB11 and GMMB10 at pockmark A

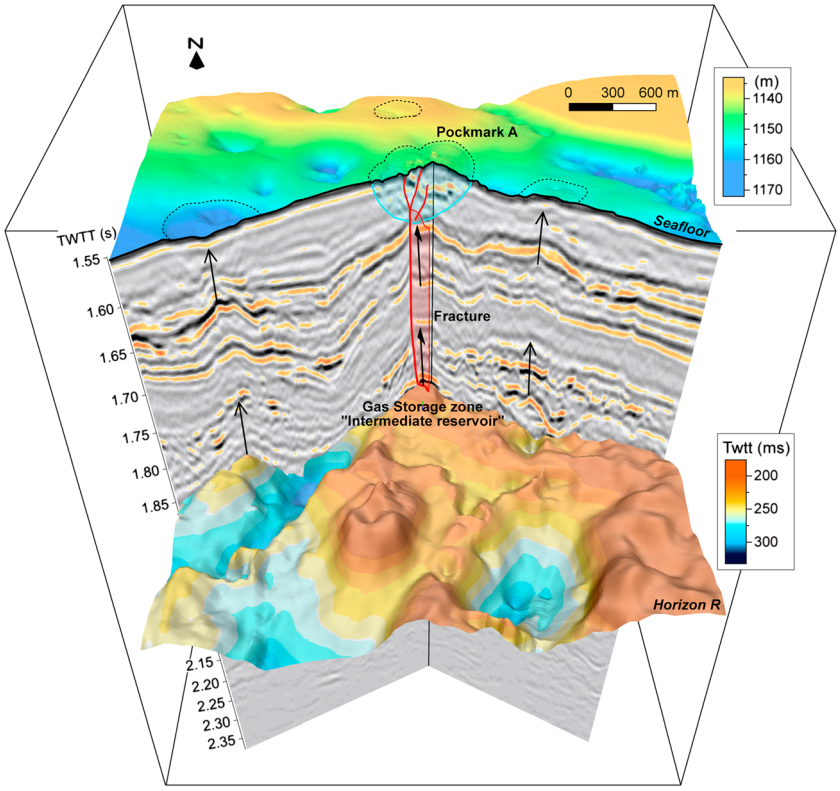

Figure 7. The 3-D cartoon crossing pockmark A and adjacent areas constructed from AUV bathymetric data and industrial 3-D seismic data showing a gas storage zone (Horizon R) at around 0.3 s (TWT) below seabed. Two other pockmarks to the east and the west of pockmark A are also supplied by gas from horizon R as indicated with black arrows but not considered further in the manuscript.

(Figures 1 and 5). The letter "G" below site GMMB11 and GMMB10 represents two other sources of free gas isolated zones (Figure 5) detected, thanks to the MeBo drillings.

An example of the correlation done between the seismic data on one hand and in situ measurements and drilling on the other hand is illustrated in Figure 8. The characterization of a high-amplitude reflector at around 15 ms (two-way travel time) below the seabed on the SYSIF profile SY01-HR-PR02 was possible, thanks to both piezocone measurements and drilling. Indeed, the cone resistance from GMPFM-11-2 shows an early refusal at 11 mbsf corresponding approximately to the top of the high-amplitude reflector (for a mean *P* wave velocity of 1450 m/s). In addition, pore water anomalies of dissolved methane (Figure 8c) and sulfate (Figure 8d) obtained from the porewater of MeBo core GMMB05 fit well with the same high-amplitude reflector. These geochemical anomalies, which are indicators of the presence of gas hydrates, will be discussed in more details later on. The use of a mean *P* wave velocity of 1450 m/s is based on direct in situ *P* wave velocity measurements acquired from the top 30 m of the sediment in the present area [*Sultan et al.*, 2007].

3.1.3.2. Interpretation

For those sites, it is clear that the source of the gas discharges corresponds to the high-amplitude anomalies observed on seismic profiles, which suggest the presence of shallow fractures in the central part of pockmark A. The presence of free gas at such shallow depth was unexpected, since the base of the GHSZ (BGHSZ) for the different sites should be located between 90 m and 120 mbsf considering the measured thermal gradient (approximately 80°C/km) [*Sultan et al.*, 2010]. The probable cause for these isolated gas pockets is rapid gas flux through fractures connected to the intermediate gas reservoir (horizon R in Figure 7).

As exemplified by the coexistence of free gas and gas hydrate at millimeter scale (see Figure 6a), the supply of large amounts of free gas by reopening or creating new fractures followed by gas hydrate formation primarily at the inner surface of such fractures leads to isolation of free gas from the surrounding pore water saturated sediment.

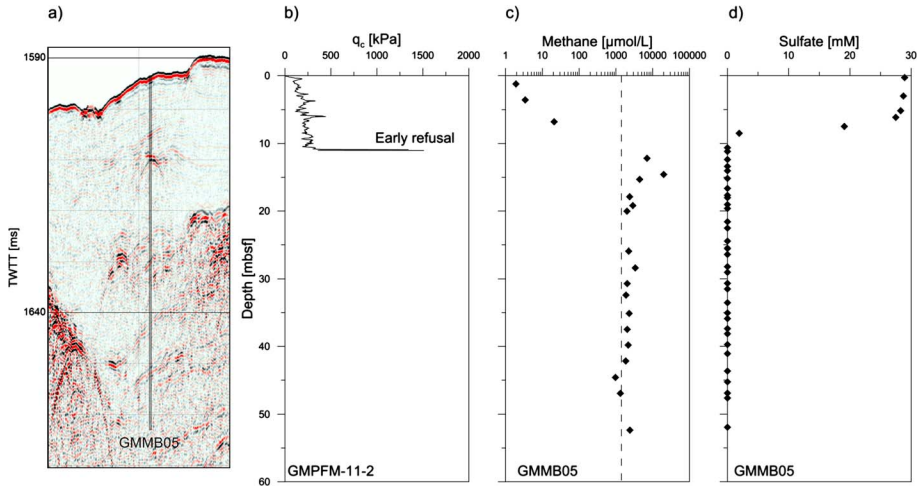

Figure 8. (a) SYSIF SY01-HR-PR02 seismic profile between SP 2000 and 2200 showing the locations of MeBo GMM05 and piezocone GMPFM-11-2. (b) Cone resistance from GMPFM-11-2 as a function of depth shows an early refusal at 11 mbsf corresponding to a high-amplitude reflector in Figure 8a. Pore water anomalies of dissolved (c) methane and (d) sulfate obtained from the pore water of MeBo core GMMB05 fit well also with high-amplitude reflector. The correlation between the seismic data and GMMB05 and GMPFM-11-2 is done for a mean *P* wave velocity of 1450 m/s.

3.1.4. Sediment Temperature and Resistance Anomalies

3.1.4.1. Previous Works and Background

Gas hydrate formation is an exothermic reaction and, thus, characterized by heat emission and a temperature increase in the surrounding sediment. In nature, gas hydrate formation is mainly controlled by molecular diffusion and fluid flow [*Wallmann et al.*, 1997]. In fine-grain sediments where the fluid flow rate is comparably low, gas dispersion is dominated by molecular diffusion [*Haeckel et al.*, 2004]. Thermal diffusivity of fine-grained marine sediments (around 10^{-6} m^2/s) [see e.g., *Waite et al.*, 2009] is several orders of magnitude higher than the molecular diffusivity of methane (10^{-12} m^2/s) [*Bigalke et al.*, 2009]. Therefore, for hydrate formation controlled by gas diffusion, temperature perturbation due to hydrate formation is expected to be negligible and most likely undetectable.

3.1.4.2. New Acquired Data and Observations

Several peak values of the corrected cone resistance (qt) indicate the presence of multiple thin gas hydrate layers at depths between 2.3 and 14.5 mbsf at site GMPFM-1-7 at the southeastern rim of pockmark A (Figures 2a and 8a). At a close-by site (GMPZ-02, Figure 2a), a piezometer was deployed to measure in situ pressure and temperature. Comparison between qt and temperature at equilibrium (Figure 8b) demonstrates that positive temperature anomalies (deviating from the average thermal gradient) correspond to the suspected two uppermost hydrate layers. Additionally, several shallow (between 1 and 2 mbsf) thermal gradient measurements in the central part of pockmark A (Figure 2a) have shown temperature anomalies with the thermal gradient exceeding 150°C/km.

3.1.4.3. Interpretation

These temperature anomalies are a clear evidence of recent hydrate formation and a clear demonstration that gas hydrate at some locations was not formed by diffusion but with a rapid free gas flux through fractures. Temperature anomalies related to upward hot fluid migration are expected to be more continuous with depth than the temperature anomalies in Figure 8b. In other terms, vertical movement of deep hot fluids is expected to cause a progressive temperature increase with depth and not peak temperature anomalies as it is observed in Figure 8.

3.2. Slow Hydrate Dissolution: Evidence From Sulfate and Methane Concentration Profiles Above the GHOZ

3.2.1. Previous Works and Background

The parameters affecting gas hydrate formation include temperature, pore pressure, gas, and pore water composition. Any variance in one of these parameters from equilibrium conditions may result in dissociation and/or dissolution of gas hydrate. Hydrate dissociation is generally caused by thermodynamic instabilities

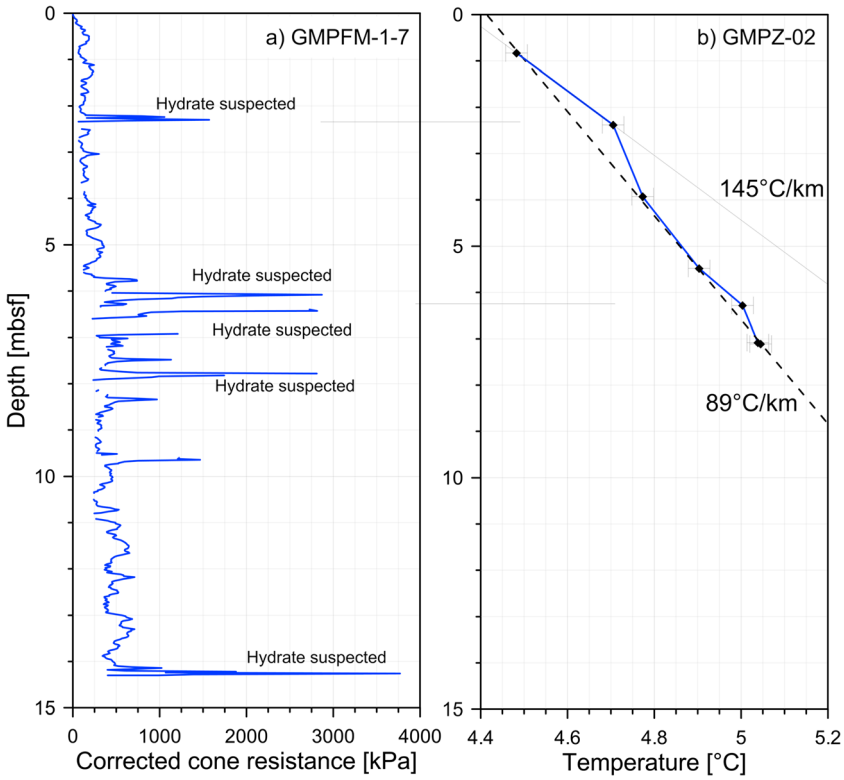

Figure 9. (a) Potential hydrate occurrence zones detected by the use of in situ piezocone measurements (site GMPF-1-7 in Figure 2a) and (b) piezometer measurements (site GMPZ-02 in Figure 2a) acquired within hydrate layers showing a thermal perturbation regime.

with the consequence of rapid release of gas-rich fluids (see for instance *Xu and Germanovich* [2006] and *Kwon et al.* [2008]). Methane hydrate dissolution occurs when hydrate comes in contact with an aqueous phase undersaturated in methane [see e.g., *Lapham et al.*, 2010]. Hydrate-bound methane will be transferred to the aqueous phase to allow new thermodynamic equilibrium conditions to be established [*Rehder et al.*, 2004; *Sultan*, 2007]. Thus, the major cause for hydrate dissolution is a deficit in dissolved methane in the surrounding pore water with dissolved methane concentrations being lower than its solubility. The sulfate-dependent anaerobic oxidation of methane (AOM) at the base of the sulfate zone contributes significantly to lower methane concentrations close to the GHOZ [*Kasten et al.*, 2012; *Iversen and Jorgensen*, 1985; *Borowski et al.*, 1996, 1999; *Hoehler et al.*, 1994]. In summary, the presence of free methane and low sulfate concentrations close to the GHOZs indicates high and rapid gas migration and/or hydrate dissociation, while extremely low methane concentrations (lower than solubility values) and high pore water sulfate concentration point to gas hydrate dissolution.

3.2.2. New Acquired Data and Observations

At drill site GMMB05 at the border of pockmark C2 (for location, see Figures 2 and 4), a high amplitude reflector at around 9.5 mbsf (Figure 4) was penetrated. This reflector was previously considered by *Sultan et al.* [2010] as an indicator for gas hydrate presence at this depth, and a gas hydrate layer has indeed been drilled at the depth of the high amplitude reflector. Infrared (IR) thermal scanning (Figure 9c) confirmed the presence of several gas hydrate layers [*Wei et al.*, 2012]. Figure 9a shows ex situ concentrations of dissolved methane versus depth at site GMMB05. Dissolved methane concentrations below the top of the GHOZ (TGHOZ) range between methane solubility at in situ pressure and temperature conditions and that at atmospheric conditions.

At the same drill site (GMMB05), pore water sulfate concentrations in the uppermost 6 m are characterized by almost constant concentrations of approximately 28 mM (Figure 9b), which is close to normal seawater concentrations. This indicates that insignificant sulfate consumption, e.g., by AOM occurs at this depth interval. Below 6 mbsf the sulfate reduction zone is encountered less than 2 m above the TGHOZ.

3.2.3. Interpretation

Methane concentrations below in situ methane solubility may be explained by gas exsolution during core recovery due to pressure decrease and potential temperature increase. Methane concentrations exceeding onboard methane solubility might be related to potential presence of microsized hydrate particles in the analyzed pore water. Moreover, concentrations of dissolved methane above the TGHOZ are several orders of magnitude lower than the methane solubility at surface conditions.

The sulfate and methane data show matching trends with dissolved methane concentrations above the TGHOZ being much lower than the methane solubility. This steep concentration gradient promotes gas hydrate dissolution from the TGHOZ. Because similar pore water sulfate and methane relations were observed at sites GMMB04 (pockmark C1), GMMB09 (off C2), GMMB03, and GMMB12 (both pockmark A), hydrate dissolution above the TGHOZ might be proposed for sites near the borders of pockmark A and pockmark cluster C as well. Gas plumes detected in the water column above the central part of pockmark A, along with the presence of shallow gas hydrate at sites GMMB10 and GMMB11, nearby prove rapid gas flux and hydrate growth in this region (Figure 6).

4. Discussion: Pockmark Formation and Evolution—The Disequilibrium Between Gas Inflow and Outflow

Previously, it was suggested that pockmark formation and evolution result from a uniform hydrate dissolution process [*Sultan et al.*, 2010]. The newly acquired data confirm that hydrate dissolution occurs in certain parts of the studied pockmarks, and gas hydrate is formed in other parts concurrently. These processes lead to a complex, heterogeneous hydrate distribution characterizing the studied pockmarks. Indeed, concurrent to hydrate dissolution, rapid hydrate growth and in some cases gas venting into the water column occurs in the most recent active parts of the pockmarks (mainly the central part of pockmark A) where gas is directly supplied through the main fracture.

Rapid hydrate growth was confirmed by multiple lines of evidence: (1) positive temperature anomalies in GHOZs (section 3.1.4), (2) free gas trapped in shallow microfractures and cracks near the surface (section 3.1.3) and released into the water column (section 3.1.2), and (3) coexistence of free gas and gas hydrate within the same sediment interval (section 3.1.1). Another possible indication for rapid gas hydrate growth induced by episodic rapid gas ascent is provided by the seismic data which imaged four successive reflectors that may correspond to hydrate/free gas fronts (reflectors F1 to F4 on SY02-HR-Pr02, Figure 4). The interpretation of reflectors F1 to F4 as hydrate/free gas fronts is based on a trial empirical calibration of a comparable seismic reflector below GMMB04 (see Figure 4). Slow hydrate dissolution, in contrast, is evident from methane concentrations being several orders of magnitude lower than the methane solubility at atmospheric temperature and pressure conditions and from the quasi-vertical sulfate profile at less than 2 m above the TGHOZs for several sites (GMMB12 and GMMB03 (both pockmark A), GMMB04 (pockmark C1), GMMB05 (pockmark C2), and GMMB09 (off pockmark C2)).

The newly acquired results also support that the first stage of pockmark formation is fluid flow from greater depth promoting subseabed hydrate accumulation. Hydrate is formed before any type of deformations affects the seafloor. This is visible from drill GMMB09 at the SE rim of pockmark C2, where hydrate and authigenic carbonate concretions were found at around 25 mbsf (SY02-HR-Pr02, Figure 4) without any deformation visible on the seabed bathymetry (Figure 2b).

Another key issue concerns the burial depth of gas hydrate occurrences in the investigated area. The maximum depth of hydrate recovered with MeBo cores was about 40 mbsf, although pore water freshening, indicative for hydrate presence, was observed at one location in deeper intervals as well.

Based on the above summarized observations, it was possible to improve the initial scheme proposed by *Sultan et al.* [2010] to describe formation and evolution of the pockmarks in the present study area. The improved scenario is described below following nine steps (Figure 10):

Step 1. (Figure 11a) Free gas accumulates and fluid pressure increases in intermediate reservoirs equivalent to horizon R in Figure 7. Once the gas pressure exceeds a critical value, free gas migrates upward while reopening annealed fractures or creating new conduits.

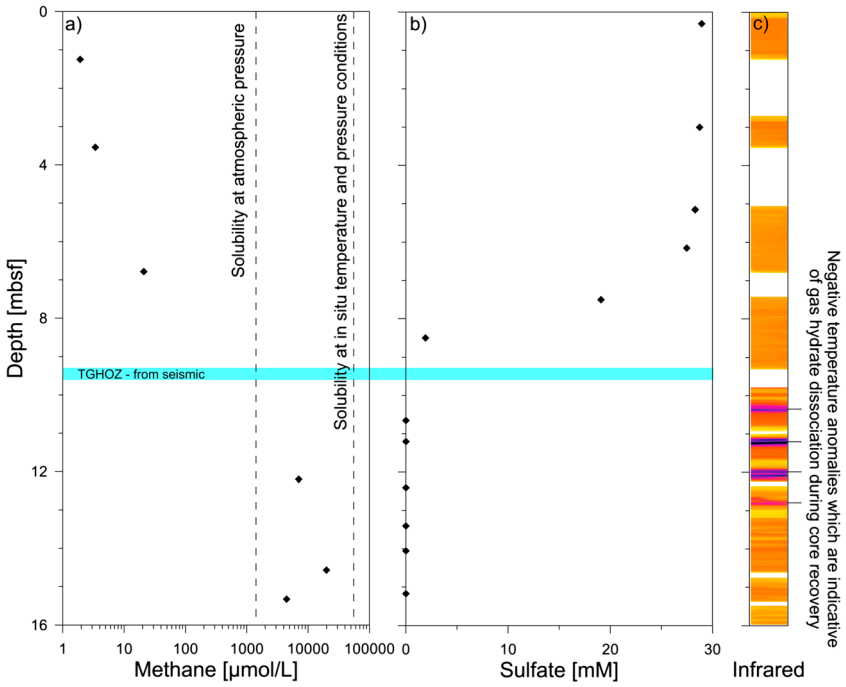

Figure 10. Pore water concentration profiles of dissolved (a) methane and (b) sulfate measured in the uppermost 16 m of MeBo core GMMB05. The shaded horizontal area illustrates the top of the GHOZ (TGHOZ) as identified from seismic data. Both methane solubilities at onboard pressure and temperature conditions as well as at in situ temperature and pressure conditions are added to Figure 10a. The measured concentrations of dissolved methane above the TGHOZ is much lower than both solubilities. The quasi-vertical sulfate profile less than 2 m above the TGHOZ corresponds to the low methane concentration above the GHOZ. (c) The infrared (IR) image shows negative temperature anomalies (purple layers) which are indicative of gas hydrate dissociation during core recovery [*Wei et al.*, 2012].

Step 2. (Figure 11a) Once the ascending free gas passes the local BGHSZ, gas hydrate is formed within the deep cohesive clay. Hydrate formation first occurs at internal surfaces of the fractured zones by creating hydrate plugs. The stiffness of the deep clays seems to be high enough to hamper lateral gas hydrate propagation. At this stage, gas hydrate may isolate free gas from the ambient pore water as it was observed during MeBo drillings. Free gas may continue at this stage to accumulate in hydrate plugs present in the GHSZ.

Step 3. (Figure 11a) The hydrate plugs are breached in case the pressure of free gas exceeds a certain value. Then, the gas can migrate into the upper package of progressively softer sediments, where lateral migration of free gas and creation of lateral fractures can take place. Gas hydrate can therefore grow into lateral direction and fill such fractures. The amount and speed of lateral gas propagation and gas hydrate formation depends mainly on the mechanical properties of the surrounding sediments. Two mechanisms can be considered for these processes (1) shallow soft sedimentary layers are pushed upward during hydrate growth and lateral fractures are created by shearing and (2) free gas pressure accumulation creates initial discontinuities, and—by stress accumulation at the border of these discontinuities—shear fractures (mode II fracture—see for instance *Rao et al.* [2003, Figure 1]) may take place. A detailed mathematical formulation of the second mechanism can be found in *Fialko et al.* [2001] and *Bunger and Detournay* [2005] where an analytical solution for this fracture propagation is obtained for pressurized horizontal circular crack in an elastic half-space.

Step 4. (Figure 11b) Free gas coexists with gas hydrate in the central part of the GHOZ. Free gas ascending from the intermediate reservoir, equivalent to horizon R in Figure 7, causes fluid overpressures and further fracturing of the upper gas hydrate cover. Elongated cap of hydrate, horizontal cracks and lateral shear discontinuities may form. Rapid hydrate growth occurs at this step causing the coexistence of free gas and gas hydrate. These successive fronts of gas hydrate formations are similar to the reflectors indicated in Figure 4 (reflectors F1 to F4).

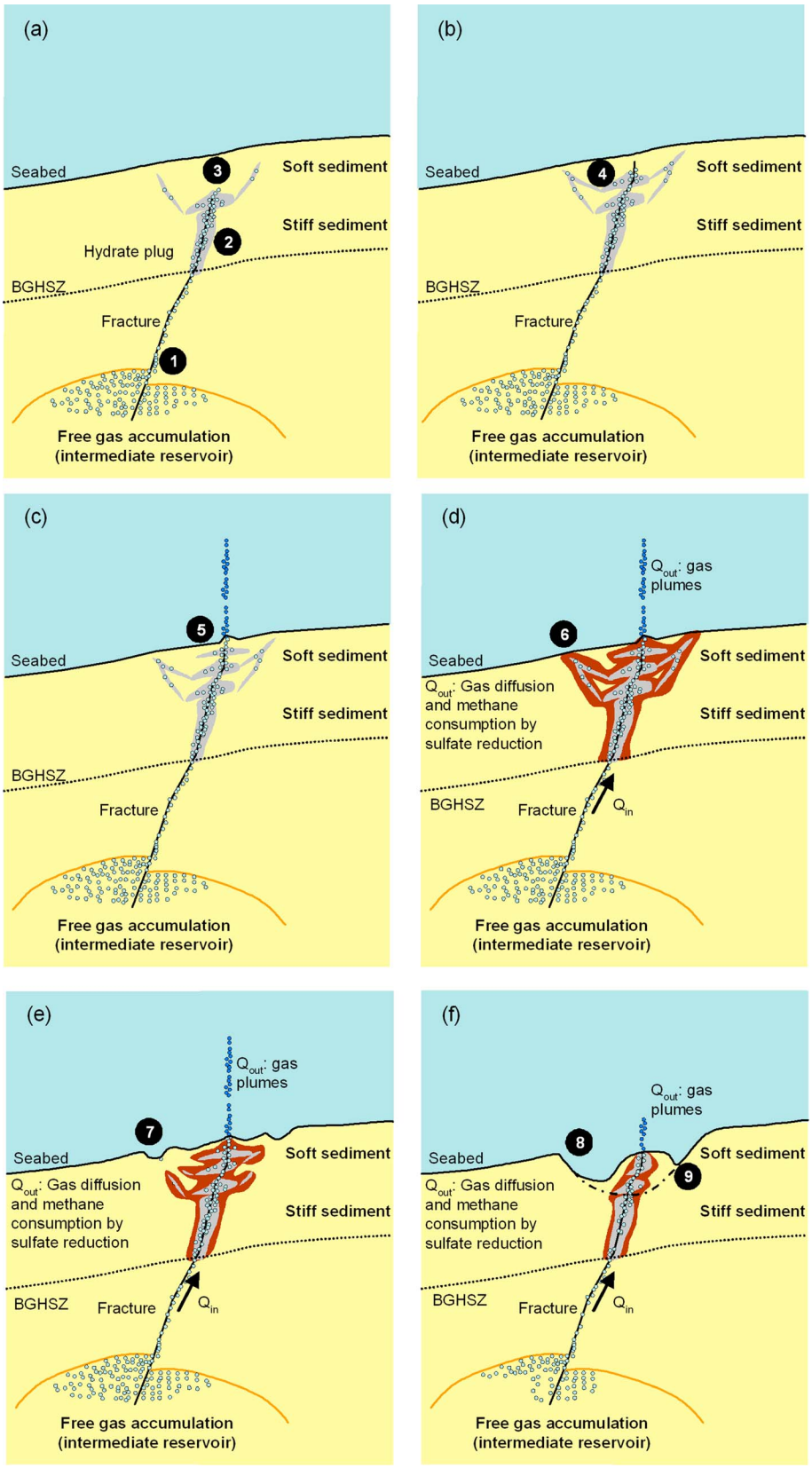

Figure 11. (a to f) Sketch of different steps in pockmark evolution during hydrate formation and dissolution (see text for details and descriptions corresponding to steps 1 to 9). Hydrate dynamics and gas (free and dissolved) inflow (Q_{in}) and outflow (Q_{out}) are the main factors controlling the pockmark formation and evolution.

Step 5. (Figure 11c)Successive elongated hydrate caps/fronts are formed in sediments shallow enough to create fractures reaching the seabed. Those fractures may constitute a direct gas migration pathway from the intermediate reservoirs to the water column. Ascent through such connections may facilitate free gas to escape into the water column as observed for the two gas plumes above pockmark A. At this step, gas fractions ascending from the reservoir are dispersed in the water column and shallow fractures, and deep faults are maintained open by the pressure of upward migrating gas.

Step 6. (Figure 11d) Coincident with rapid hydrate formations in near-vertical fractures, lateral discontinuities, and shear bands, hydrate dissolution occurs at the outer limits of the GHOZ (brown contours in Figures 10d–10f). Indeed, the long-term occurrence of hydrate close to the seafloor must be sustained by gas supply sufficient to maintain boundary layer saturation or even continuous hydrate growth [*Rehder et al.*, 2004]. The huge amount of free gas migrating rapidly almost instantaneously by successive episodes is at the origin of hydrate saturated cracks, shear bands, and fractures. The long-term occurrence of such gas hydrate layers and discontinuities can only be maintained by sufficient supply of gas. Therefore, hydrate formation and dissolution are controlled by the balance between gas inflow (Q_{in}) from the intermediate reservoirs and gas outflow (Q_{out}) including hydrate dissolution at the border of the GHOZ sustained by AOM and gas plumes in the water column. Moreover, rapid formation of gas hydrate slabs and plugs limits significantly lateral gas migration which is required to sustain hydrate stability at the borders of hydrate-bearing zones.

Step 7. (Figure 11e) Due to the obvious differences in gas inflow (Q_{in}) and outflow (Q_{out}) rates and to the low permeability of hydrate-bearing zones for free gas migration, dissolution of gas hydrate and disappearance of hydrate slabs and plugs commences at the border of the GHOZ. As a consequence, a circular collapse structure surrounding the central gas hydrate-rich zone is formed as indicated by the subcircular depressions in the shaded bathymetry in Figure 1.

Step 8. (Figure 11f) Hydrate dissolution is a function of the deficit between Q_{in} and Q_{out} and proceeds from the borders of the GHOZ (brown areas in Figure 10f). The material loss due to hydrate dissolution is accompanied by a deepening of the pockmark rim with a preservation of a dome-like structure in the pockmark center due to the preservation of hydrate adjacent to the free gas conduit. A central dome-like structure is suggested by the seafloor morphology to the south of pockmark C3 (Figure 2b).

Step 9. (Figure 11f) The final stage is caused by interruption of upward gas migrations from the intermediate reservoir. This may lead to complete dissolution of hydrate in near-surface sediments and decay of the central dome-like structure. This may be accompanied by formation of a relatively regular pockmark, for example, pockmark B shown in Figure 1.

The process sequences described above are based on recent observations but remain conceptual. For instance, the time factor controlling the different mechanisms is unknown. In order to verify the scheme presented in Figure 10, a more comprehensive and quantitative overview on short- and long-term processes that shape pockmarks in the present area is necessary with a need to carry out

1. Pore water analyses of dissolved gas and sulfate concentrations in sediments surrounding the GHOZ at selected pockmarks allowing modeling the short-term dynamics of gas hydrate in this area [see for more details *Malinverno et al.* 2008 and *Bhatnagar et al.*, 2007].
2. U/Th dating of authigenic cold seep carbonates which may reveal the dynamic of gas flux over the last few thousand years at selected pockmarks [*Bayon et al.*, 2009; *Feng et al.*, 2010].

5. Conclusion

In the present work, it is shown that rapid gas hydrate growth and slow hydrate dissolution are the main mechanisms affecting seabed pockmarks and subseabed facies architecture observed in the study area. Gas hydrate forms through rapid gas migration, as confirmed by in situ positive temperature anomalies, free gas trapped in shallow microfractures in the GHOZ, and the coexistence between free gas and gas hydrate. At the same time, gas hydrate dissolves relatively slowly due to the methane deficit in the surrounding sediment, where concentrations of dissolved methane are below solubility. The pore water sulfate reduction zone is

limited due to low methane concentrations surrounding gas hydrate (less than 2 m above the GHOZ). Therefore, based on the above observations and on detailed analyses of seabed and subseabed structures, an update of the scenario by *Sultan et al.* [2010] is proposed to describe formation and evolution of the pockmarks in deep water Nigeria.

In conclusion, this work shows that localized gas migration through the center of the GHOZ can coexist with methane deficit at the periphery of the same pockmark. It also provides further evidence about the role of hydrate dissolution for sediment deformations in the GHSZ.

Acknowledgments

The support by officers and crew during Guineco-MeBO cruises is greatly appreciated, as is the dedication of the technical staff during the cruise. Constructive comments by Christian Berndt, Andreia Plaza-Faverola, and the Associate Editor helped improve the manuscript significantly. Additionally, we would like to acknowledge our industrial partner, Total, for providing a part of the used data. Data used in the present paper are covered by a confidentiality agreement between Total, Ifremer, and Marum that restrict access; interested readers can contact the authors for more information.

References

Abegg, F., H. J. Hohnberg, T. Pape, G. Bohrmann, and J. Freitag (2008), Development and application of pressure-core-sampling systems for the investigation of gas- and gas-hydrate-bearing sediments, *Deep Sea Res., Part I*, *55*(11), 1590–1599, doi:10.1016/j.dsr.2008.06.006.

Bayon, G., G. M. Henderson, and M. Bohn (2009), U-Th stratigraphy of a cold seep carbonate crust, *Chem. Geol.*, *260*(1-2), 47–56, doi:10.1016/j.chemgeo.2008.11.020.

Bhatnagar, G., W. G. Chapman, G. R. Dickens, B. Dugan, and G. J. Hirasaki (2007), Generalization of gas hydrate distribution and saturation in marine sediments by scaling of thermodynamic and transport processes, *Am. J. Sci.*, *307*(6), 861–900, doi:10.2475/06.2007.01.

Bigalke, N. K., G. Rehder, and G. Gust (2009), Methane hydrate dissolution rates in undersaturated seawater under controlled hydrodynamic forcing, *Mar. Chem.*, *115*(3-4), 226–234, doi:10.1016/j.marchem.2009.09.002.

Borowski, W. S., C. K. Paull, and W. Ussler (1996), Marine pore-water sulfate profiles indicate in situ methane flux from underlying gas hydrate, *Geology*, *24*(7), 655–658, doi:10.1130/0091-7613(1996)024<0655:mpwspi>2.3.co;2.

Borowski, W. S., C. K. Paull, and W. Ussler (1999), Global and local variations of interstitial sulfate gradients in deep-water, continental margin sediments: Sensitivity to underlying methane and gas hydrates, *Mar. Geol.*, *159*(1-4), 131–154.

Bunger, A. P., and E. Detournay (2005), Asymptotic solution for a penny-shaped near-surface hydraulic fracture, *Eng. Fract. Mech.*, *72*(16), doi:10.1016/j.engfracmech.2005.06.005.

Feng, D., H. H. Roberts, H. Cheng, J. Peckmann, G. Bohrmann, R. L. Edwards, and D. Chen (2010), U/Th dating of cold-seep carbonates: An initial comparison, *Deep Sea Res., Part II*, *57*(21-23), 2055–2060, doi:10.1016/j.dsr2.2010.09.004.

Fialko, Y., Y. Khazan, and M. Simons (2001), Deformation due to a pressurized horizontal circular crack in an elastic half-space, with applications to volcano geodesy, *Geophys. J. Int.*, *146*(1), doi:10.1046/j.1365-246X.2001.00452.x.

Freudenthal, T., G. Wefer, and IEEE (2009), *Shallow Drilling in the Deep Sea: The Sea Floor Drill Rig MEBO, Oceans 2009 - Europe*, vol. 1, 2, pp. 180–183, IEEE, New York.

Georges, R. A., and E. Cauquil (2007), AUV ultrahigh-resolution 3D seismic technique for detailed subsurface investigations, Offshore Technology Conference, Houston, OTC18784.

Haeckel, M., E. Suess, K. Wallmann, and D. Rickert (2004), Rising methane gas bubbles form massive hydrate layers at the seafloor, *Geochim. Cosmochim. Acta*, *68*(21), 4335–4345, doi:10.1016/j.gca.2004.01.018.

Hoehler, T. M., M. J. Alperin, D. B. Albert, and C. S. Martens (1994), Field and laboratory studies of methane oxidation in an anoxic marine sediment: Evidence for a methanogen-sulfate reducer consortium, *Global Biogeochem. Cycles*, *8*, 451–463.

Iversen, N., and B. B. Jorgensen (1985), Anaerobic methane oxidation rates at the sulphate methane transition in marine-sediments from Kattegat and Skagerrak (Denmark), *Limnol. Oceanogr.*, *30*(5), 944–955.

Kasten, S., K. Noethen, C. Hensen, V. Spiess, M. Blumenberg, and R. R. Schneider (2012), Gas hydrate decomposition recorded by authigenic barite at pockmark sites of the northern Congo Fan, *Geo Mar. Lett.*, *32*(5-6), 515–524, doi:10.1007/s00367-012-0288-9.

Ker, S., B. Marsset, S. Garziglia, Y. Le Gonidec, D. Gibert, M. Voisset, and J. Adamy (2010), High-resolution seismic imaging in deep sea from a joint deep-towed/OBH reflection experiment: Application to a Mass Transport Complex offshore Nigeria, *Geophys. J. Int.*, *182*, 1524–1542.

Kwon, T. H., G. C. Cho, and J. C. Santamarina (2008), Gas hydrate dissociation in sediments: Pressure-temperature evolution, *Geochem. Geophys. Geosyst.*, *9*, Q03019, doi:10.1029/2007GC001920.

Lapham, L. L., J. P. Chanton, R. Chapman, and C. S. Martens (2010), Methane under-saturated fluids in deep-sea sediments: Implications for gas hydrate stability and rates of dissolution, *Earth Planet. Sci. Lett.*, *298*, 275–285, doi:10.1016/j.epsl.2010.07.016.

Lee, M. W., and T. S. Collett (2006), Gas hydrate and free gas saturation estimated from velocity logs on Hydrate Ridge, offshore Oregon, U.S.A., in *Proc Ocean Drill Program Sci Results*, vol. 204, edited by A. M. Trehu et al., 1–25, Proc. Ocean Drill Program Sci. Results, College Station, Tex.

Liu, X. L., and P. B. Flemings (2006), Passing gas through the hydrate stability zone at southern Hydrate Ridge, offshore Oregon, *Earth Planet. Sci. Lett.*, *241*(1-2), 211–226, doi:10.1016/j.epsl.2005.10.026.

Malinverno, A., M. Kastner, M. E. Torres, and U. G. Wortmann (2008), Gas hydrate occurrence from pore water chlorinity and downhole logs in a transect across the northern Cascadia margin (Integrated Ocean Drilling Program Expedition 311), *J. Geophys. Res.*, *113*, B08103, doi:10.1029/2008JB005702.

Marsset, T., B. Marsset, S. Ker, Y. Thomas, and Y. Le Gall (2010), High and very high resolution deep-towed seismic system: Performance and examples from deep water geohazard studies, *Deep Sea Res., Part I*, doi:10.1016/j.dsr.2010.01.001.

Milkov, A. V., G. R. Dickens, G. E. Claypool, Y. J. Lee, W. S. Borowski, M. E. Torres, W. Y. Xu, H. Tomaru, A. M. Trehu, and P. Schultheiss (2004), Co-existence of gas hydrate, free gas, and brine within the regional gas hydrate stability zone at Hydrate Ridge (Oregon margin): Evidence from prolonged degassing of a pressurized core, *Earth Planet. Sci. Lett.*, *222*(3-4), 829–843, doi:10.1016/j.epsl.2004.03.028.

Pape, T., A. Bahr, S. A. Klapp, F. Abegg, and G. Bohrmann (2011), High-intensity gas seepage causes rafting of shallow gas hydrates in the southeastern Black Sea, *Earth Planet. Sci. Lett.*, *307*(1-2), doi:10.1016/j.epsl.2011.04.030.

Paull, C. K., W. Ussler, W. S. Borowski, and F. N. Spiess (1995), Methane-rich plumes on the Carolina continental rise – associations with gas hydrates, *Geology*, *23*(1), doi:10.1130/0091-7613(1995)023<0089:mrpotc>2.3.co;2.

Rao, Q. H., Z. Q. Sun, O. Stephansson, C. L. Li, and B. Stillborg (2003), Shear fracture (Mode II) of brittle rock, *Int. J. Rock Mech. Min. Sci.*, *40*(3), doi:10.1016/s1365-1609(03)00003-0.

Rehder, G., S. H. Kirby, W. B. Durham, L. A. Stern, E. T. Peltzer, J. Pinkston, and P. G. Brewer (2004), Dissolution rates of pure methane hydrate and carbon-dioxide hydrate in undersaturated seawater at 1000-m depth, *Geochim. Cosmochim. Acta*, *68*(2), 285–292, doi:10.1016/j.gca.2003.07.001.

Roemer, M., H. Sahling, T. Pape, G. Bohrmann, and V. Spiess (2012), Quantification of gas bubble emissions from submarine hydrocarbon seeps at the Makran continental margin (offshore Pakistan), *J. Geophys. Res.*, *117*, C10015, doi:10.1029/2011JC007424.

Sultan, N. (2007), Comment on "Excess pore pressure resulting from methane hydrate dissociation in marine sediments: A theoretical approach" by Wenyue Xu and Leonid N. Germanovich, *J. Geophys. Res.*, *112*, B02103, doi:10.1029/2006JB004527.

Sultan, N., M. Voisset, T. Marsset, A. M. Vernant, E. Cauquil, J. L. Colliat, and V. Curinier (2007), Detection of free gas and gas hydrate based on 3D seismic data and cone penetration testing: An example from the Nigerian Continental Slope, *Mar. Geol.*, *240*(1-4), 235–255, doi:10.1016/j.margeo.2007.02.012.

Sultan, N., et al. (2010), Hydrate dissolution as a potential mechanism for pockmark formation in the Niger delta, *J. Geophys. Res.*, *115*, B08101, doi:10.1029/2010JB007453.

Taylor, M. H., W. P. Dillon, and I. A. Pecher (2000), Trapping and migration of methane associated with the gas hydrate stability zone at the Blake Ridge Diapir: New insights from seismic data, *Mar. Geol.*, *164*(1-2), doi:10.1016/s0025-3227(99)00128-0.

Torres, M. E., K. Wallmann, A. M. Trehu, G. Bohrmann, W. S. Borowski, and H. Tomaru (2004), Gas hydrate growth, methane transport, and chloride enrichment at the southern summit of Hydrate Ridge, Cascadia margin off Oregon, *Earth Planet. Sci. Lett.*, *226*(1-2), 225–241, doi:10.1016/j.epsl.2004.07.029.

Trehu, A. M., et al. (2003), Proc. ODP, Initial reports, 204, Ocean Drilling Program, College Station, TX. doi:10.2973/odp.proc.ir.204.2003.

Waite, W. F., et al. (2009), Physical properties of hydrate-bearing sediments, *Rev. Geophys.*, *47*, RG4003, doi:10.1029/2008RG000279.

Wallmann, K., P. Linke, E. Suess, G. Bohrmann, H. Sahling, M. Schluter, A. Dahlmann, S. Lammers, J. Greinert, and N. von Mirbach (1997), Quantifying fluid flow, solute mixing, and biogeochemical turnover at cold vents of the eastern Aleutian subduction zone, *Geochim. Cosmochim. Acta*, *61*(24), doi:10.1016/s0016-7037(97)00306-2.

Wei, J. G., G. Bohrmann, N. Sultan, T. Himmler, T. Pape, B. Dennielou, L. Ruffine, S. Garziglia, and the GUINECO-MeBo shipboard scientific party (2012), Distribution of gas hydrates in submarine pockmark deposits of the Nigerian margin inferred from infrared thermal core scanning, Processes and Products, 24-28 September 2012. Hamburg, Germany.

Xu, W. Y., and L. N. Germanovich (2006), Excess pore pressure resulting from methane hydrate dissociation in marine sediments: A theoretical approach, *J. Geophys. Res.*, *111*, B01104, doi:10.1029/2004JB003600.